Polarizable atomic multipole X-ray refinement: weighting schemes for macromolecular diffraction

**T. D. Fenn[a]* and
M. J. Schnieders[b]**

[a]Department of Bioengineering, Stanford University, Stanford, California, USA, and [b]Department of Biomedical Engineering, University of Texas, Austin, Texas, USA

Correspondence e-mail: fenn@stanford.edu

In the past, weighting between the sum of chemical and data-based targets in macromolecular crystallographic refinement was based on comparing the gradients or Hessian diagonal terms of the two potential functions. Here, limitations of this scheme are demonstrated, especially in the context of a maximum-likelihood target that is inherently weighted by the model and data errors. In fact, the congruence between the maximum-likelihood target and a chemical potential based on polarizable atomic multipole electrostatics evaluated with Ewald summation has opened the door to a transferable static weight. An optimal static weight is derived from first principles and is demonstrated to be transferable across a broad range of data resolutions in the context of a recent implementation of X-ray crystallographic refinement using the polarizable AMOEBA force field and it is shown that the resulting models are balanced with respect to optimizing both R_{free} and *MolProbity* scores. Conversely, the classical automatic weighting scheme is shown to lead to underfitting or overfitting of the data and poor model geometry. The benefits of this approach for low-resolution diffraction data, where the need for prior chemical information is of particular importance, are also highlighted. It is demonstrated that this method is transferable between low- and high-resolution maximum-likelihood-based crystallographic refinement, which proves for the first time that resolution-dependent parameterization of either the weight or the chemical potential is unnecessary.

1. Introduction

Crystallographic refinement of atomic coordinates involves optimization against both a chemical potential energy (or force field, $E_{\mathrm{ForceField}}$) and the observed data $E_{\mathrm{X\text{-}ray}}$,

$$E_{\mathrm{tot}} = E_{\mathrm{ForceField}} + w_{\mathrm{A}} E_{\mathrm{X\text{-}ray}}, \qquad (1)$$

where w_{A} weights the data relative to the force-field component. We assume throughout that weighting of other parameters, such as occupancies and B factors, is independent of coordinates. Also, we do not consider the case of additional experimental information such as neutron or real-space data, although much of what is discussed below is also applicable to these cases (see, for example, Fenn *et al.*, 2011). A widely adopted standard for determining an optimal w_{A} involves calculating the ratio of the gradient norms between the two objective functions,

$$w_A = \frac{||\nabla E_{\text{ForceField}}||}{||\nabla E_{\text{X-ray}}||} \qquad (2)$$

as originally described by Brünger (1988) and standardized over the course of several years (Wang & Stubbs, 1993; Adams *et al.*, 1997). Therefore, if the X-ray gradient is smaller than the chemical gradient on average, it is upweighted to balance the two potentials and *vice versa* (Fig. 1).

The standard formalism for the $E_{\text{X-ray}}$ term in (1) as it is applied to macromolecular structures utilizes a likelihood target (hereafter referred to as 'crystallographic likelihood') that includes both data and model error. The latter is accounted for by inflating the total variance and down-weighting the model contribution owing to incompleteness and coordinate error [the full details of the likelihood target will not be discussed here; the reader is referred to McCoy (2004) and references therein for a more thorough discussion], causing the likelihood to become less peaked and broader as the model error increases. A similar method of weighting the data is common in model refinement in the context of NMR (Habeck *et al.*, 2006).

The crystallographic likelihood can be stated as the probability of observing the measured data (D) given an atomic model (X). This can be formally written as a conditional probability $p(D|X)$. However, what we seek to optimize is the probability of the atomic model given the measured data, $p(X|D)$. This is accomplished through Bayes' rule,

$$p(X|D) \propto p(D|X)p(X), \qquad (3)$$

where $p(X)$ represents the prior probability of the atomic model based on our established understanding of molecular energetics. Although computational solutions to the Schrödinger equation (*i.e.* quantum mechanics) are the gold standard for molecular energetics, *ab initio* electronic structure calculations that use a reliable basis set and account for electron correlation are prohibitively expensive for macromolecular refinement. For this reason, a modern polarizable force field, such as AMOEBA, that accurately reproduces the quantum-mechanical potential energy surface is the most compelling alternative for prior chemical information (Ponder *et al.*, 2010; Ren *et al.*, 2011).

The relative probability of an atomic conformation is given by its Boltzmann factor $\exp[-U(X)/kT]$ and therefore (3) can be expressed as

$$p(X|D) \propto p(D|X)\exp[-U(X)/kT], \qquad (4)$$

where $U(X)$ is the potential energy of the crystal according to a polarizable force field. For convenience, the maximum of $p(X|D)$ is determined by minimization of its negative logarithm, which yields a hybrid energy function for the model $E(X)$,

$$E(X) = -\log[p(D|X)] + U(X)/kT. \qquad (5)$$

This is identical to the form presented initially in (1) and identifies $w_A = kT$ as the expected value of the weight to apply to the crystallographic likelihood to balance the two terms. At 300 K, kT equals 0.6 (on a kcal mol^{-1} scale) such that if the prior chemical information is of high quality then weights close to 0.6 are expected to balance model agreement with respect to both the observed data (*i.e.* R_{free}) and prior chemical knowledge (*i.e. MolProbity* score).

Independent of the target type used, the effect of (2) tends to upweight the weaker (flatter) potential, which may not be desirable if the weaker potential is associated with low confidence. To illustrate this, in the extreme case of subatomic resolution (>1.0 Å) data, the crystallographic likelihood and its derivatives will be sharply defined (illustrated by the red curve in Fig. 1c). The effect of (2), in this case, will be to downweight the data (indicated by the transition from Fig. 1c to Fig. 1b). If the potential wells are not congruous, this will cause the coordinates to move away from the well determined data-based target and towards the chemical prior potential 'well'. Likewise, in the opposing extreme of poor data, the crystallographic likelihood will be relatively flat (red curve in Fig. 1a). (2) will have the effect of upweighting the data in this case, causing the atoms to move away from the chemical prior 'well' and towards the uncertain X-ray potential 'well' (indicated in Fig. 1 by the transition from Fig. 1a to Fig. 1b). The resulting effect of this scheme will cause low-resolution data sets to be overweighted, yielding models with poor geometry and potentially increased R_{free} values owing to overfitting. Conversely, high-resolution data sets will be downweighted, leading to inflated R and R_{free} values and models with
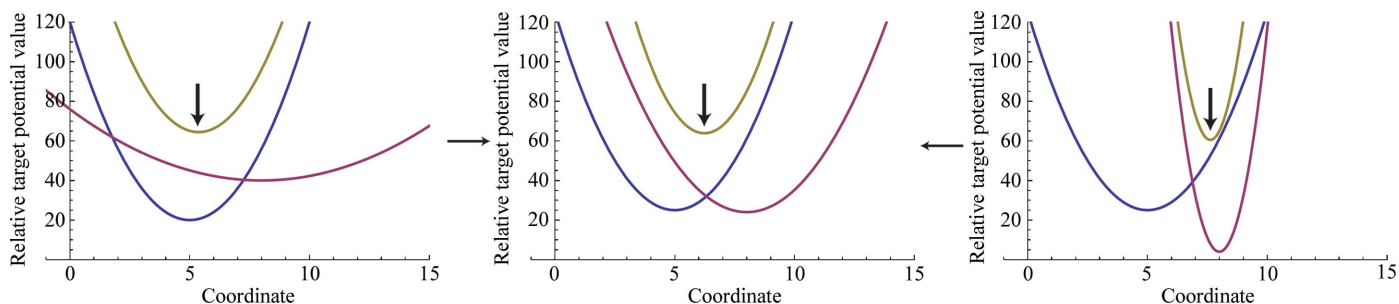
Figure 1
The effect of no weighting on X-ray (red) and chemical (blue) potentials in noncongruous cases, with the total potential shown in yellow. The global minimum is marked by a thick downward-pointing arrow in each case. In the case of low-resolution or poorly measured X-ray data (*a*), the X-ray potential will be weakly defined and the minima will favor the chemical potential. Alternatively, in the case of well measured or high-resolution X-ray data (*c*), the X-ray potential will be sharp and cause the minima to favor the data. The effect of equation (2) is to bring these two potentials onto the same scale as the chemical potential (*b*).

conservative geometry. This may partly explain the noted correlation between data resolution and measures of model quality (Arendall *et al.*, 2005; Bhattacharya *et al.*, 2007). While options exist to test a variety of w_A values, the default behavior in most likelihood-based refinement packages is to utilize the mechanism in (2), which may partly be a consequence of limitations in the force fields commonly used in crystallographic refinement, as also suggested by McCoy (2004).

Ideally, the force field and data-based target will be congruent: *i.e.* the minima for the two objective functions describing these terms are equivalent and the weighting between them is therefore less critical. It is reasonable to hypothesize that the degree of overlap/agreement should correlate with the level of detail used in describing the molecular physics of the chemical system. For example, models that take into account charge interactions of ions with their full environment (including long-range interactions), polarization, bond–angle coupling effects *etc.* will more accurately reproduce the atomic forces within the crystal. Our previous work illustrated an improved congruence between the polarizable AMOEBA force field and the crystallographic target (Schnieders *et al.*, 2011) with less dependence on the weighting scheme for a variety of resolutions and data qualities. Further, the benefit of refining against higher quality biomolecular physics (*i.e.* a polarizable atomic multipole force field) has been shown in several X-ray and neutron crystallographic contexts (Schnieders *et al.*, 2009; Fenn, Schnieders, Brunger *et al.*, 2010; Fenn *et al.*, 2011). However, it is important to point out that even the most modern approaches fail to recognize that crystal conformations are governed by free energy rather than potential energy. Optimization based on a potential energy is equivalent to quenching the crystal to 0 K. Future work is needed to incorporate entropic effects into the prior probability of the model during crystallographic refinement, similar to efforts made in the protein-folding field (Faver *et al.*, 2011).

Here, we have sought to more extensively test the effect of weighting on the resultant *R* values and model geometry using our recently developed molecular-physics platform called *Force Field X* (*FFX*) that executes within the Java Runtime Environment (JRE). This includes an implementation of the atomic multipole optimized energetics for biomolecular applications (AMOEBA) force field (Ren & Ponder, 2003, 2004; Ponder *et al.*, 2010; Ren *et al.*, 2011), a particle mesh Ewald (PME) method (Darden *et al.*, 1993; Essmann *et al.*, 1995; Sagui *et al.*, 2004) using shared memory parallelization and symmetry operators for efficient computation of electrostatic energies (Schnieders *et al.*, 2011) and a crystallographic likelihood target using a differentiable bulk-solvent model (Fenn, Schnieders & Brunger, 2010). By re-refining 18 macromolecular models spanning a range of resolutions, we show the agreement between the chemical and crystallographic potentials achieves a good balance – and is typically optimized in both cases – by scaling the X-ray component using a w_A value close to *kT*. In effect, the maximum-likelihood target and prior chemical information are both in units of kcal mol^{-1}, which has the advantage of aiding

chemical interpretation of model improvements. This suggests rigorous molecular physics coupled with crystallographic likelihood does not require resolution-dependent or data-quality-dependent weighting schemes. We also illustrate the effects of automatic weighting and its potential pitfalls.

2. Methods

Testing was performed on 18 structures selected from the PDB to encompass a variety of starting model qualities as determined from *MolProbity* scores (Chen *et al.*, 2010) and a broad resolution range. The PDB entries selected based on these criteria were 3bbw, 3crw, 2r4r, 1a7b, 1bl8, 3ffn, 2quk, 2fnp, 3g8l, 1sfc, 3et9, 2r0f, 3gpn, 1mhq, 3o7h, 1dp0, 2ipr and 2rk4.

Models were prepared by using the *CNS* `generate.inp` script, which carries out a brief Cartesian dynamics step (50 steps of 5 fs each) and adds H atoms if necessary to the input coordinates. The model generated in this fashion was then used as input for one of four different refinement methodologies. The first involved using an OPLS-AA-X force field with electrostatics computed using a spherical cutoff of 8.5 Å (with a switching function that begins taking effect at 6.5 Å) and the CHARM22 version of the TIP3P water model as implemented in *CNS* v.1.3 (Jorgensen & Tirado-Rives, 1988; Engh & Huber, 1991; Linge *et al.*, 2003; Nozinovic *et al.*, 2010; Schröder *et al.*, 2010; Fenn *et al.*, 2011). The weight w_A was set to either 1.0 or left to the automatic setting as per (2). Only local optimization was performed based on three macrocyles of refinement which included 150 coordinate and 100 *B*-factor minimization steps. The second and third refinement methodologies utilized *PHENIX* v.1.6.4 and *REFMAC* v.5.0109, respectively, which include an Engh and Huber restraint set based on the CIF dictionary model (Engh & Huber, 1991; Vagin *et al.*, 2004; Adams *et al.*, 2010) and no treatment of electrostatics. For the *PHENIX* refinements, three macrocycles of 150 maximum iterations were performed and weights were fixed at 1.0 or determined automatically. For the *REFMAC*-based refinements, 50 cycles of combined coordinate and *B*-factor optimization were performed using automatic weighting only (using the 'weight auto' option). An appropriate static weight for each model was not determined for the *REFMAC* refinements, as there is no standard method for its determination. None of the refinement methods employed additional restraints (*e.g.* hydrogen bond, NCS, Ramachandran restraints *etc.*) other than the default parameterizations encoded in the programs.

The fourth refinement method involved our recently described *FFX* platform (Fenn, Schnieders & Brunger, 2010; Schnieders *et al.*, 2011). The chemistry term in *FFX* is based on the AMOEBA force field (Ren & Ponder, 2003, 2004; Ponder *et al.*, 2010; Ren *et al.*, 2011) with electrostatics computed using a symmetrized particle-mesh Ewald approach (Sagui *et al.*, 2004; Schnieders *et al.*, 2011). The X-ray term is based on the maximum-likelihood model determined using spline coefficients (Murshudov *et al.*, 1997; Cowtan, 2002, 2005) and the methodology of Fenn for derivatives with respect to atomic coordinates and bulk solvent (Brünger, 1989; Fenn,

research papers

Schnieders & Brunger, 2010). The bulk solvent itself was modeled using a differentiable polynomial switch model (Fenn, Schnieders & Brunger, 2010). Electron density for the atomic model was computed using the isolated-atom formalism as described by Schnieders *et al.* (2009). Structure factors for both terms were computed using fast Fourier methods (Ten Eyck, 1973, 1977) and symmetry was applied in reciprocal space if necessary (Waser, 1955; Brünger, 1989) using the recommendations of Bricogne for sampling and symmetrization of structure factors (Bricogne, 2006). Fitting of scale factors between the model and data structure-factor amplitudes are based on the methods of Afonine *et al.* (2005*b*). Local optimizations were performed to an r.m.s. gradient convergence of 0.1 kcal mol^{-1} Å^{-1} and *B*-factor optimizations were converged to an r.m.s. gradient of 0.01 (unitless).

Following refinement, models were analyzed using *MolProbity* (Chen *et al.*, 2010) and hydrogen bonds were tabulated and analyzed (*e.g.* for computation of the percentage of hydrogen bonds; Table 1) using the *Hydrogen Bond Analysis Tool* (*HBAT*; Panigrahi & Desiraju, 2007).
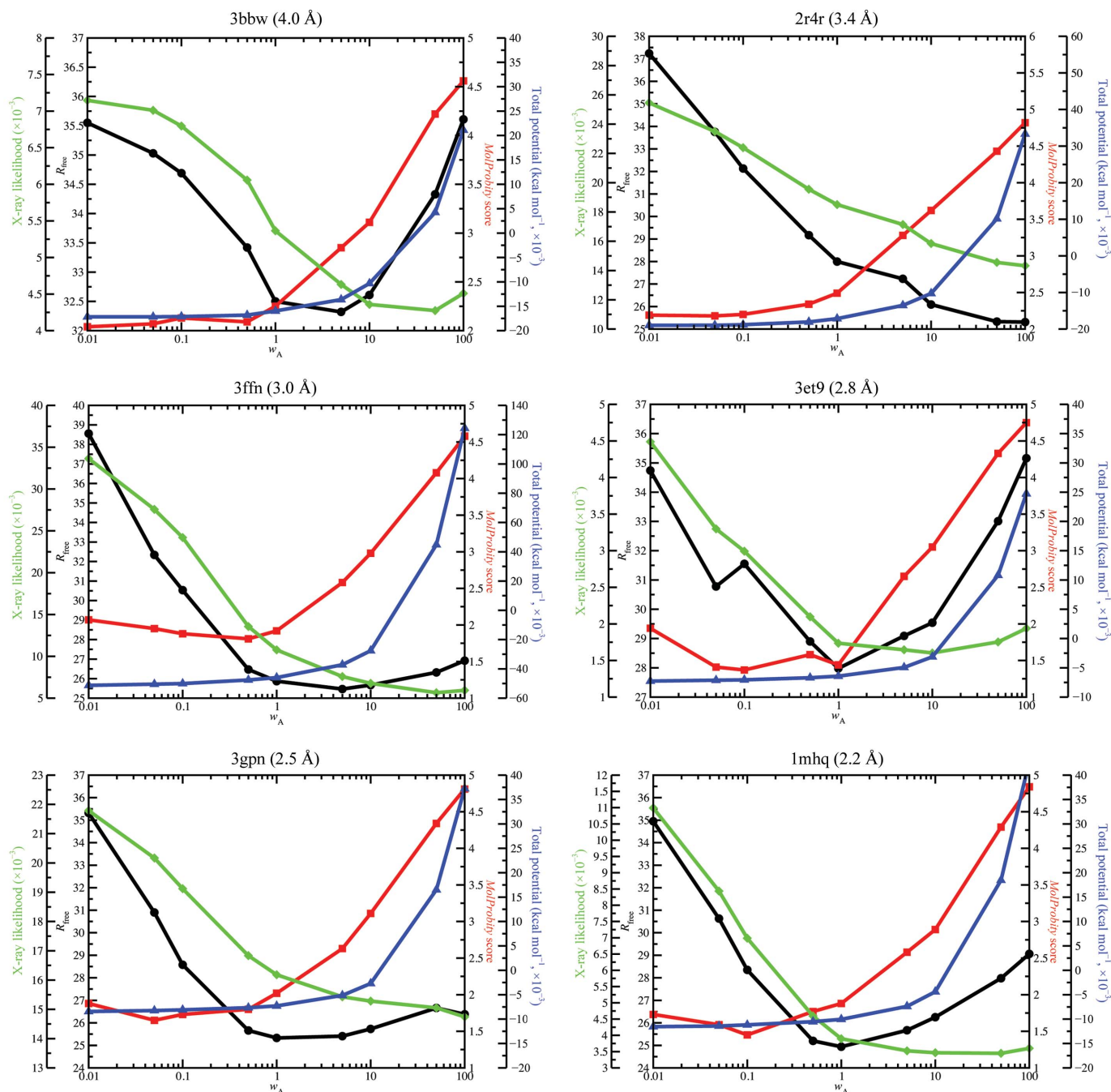
Figure 2
Plot of R_{free} (left *y* axis; black), total X-ray potential (second left *y* axis; green), *MolProbity* scores (right *y* axis; red) and total chemical potential (second right *y* axis; blue) *versus* w_{A} (logarithmic scale) for six representative structures ranging from 2.2 to 4.0 Å resolution (PDB codes and resolutions are given above each respective plot).

3. Results

To determine optimum weights for *FFX*, we initially performed a grid search centered around a w_A of 1.0 for 18 different structures spanning diffraction limits of 1.2–4.0 Å resolution. Representative plots for ten of these structures in terms of R_{free}, *MolProbity* score and the total chemical and X-ray targets as a function of w_A are illustrated in Figs. 2 and 3. Briefly, the *MolProbity* score of a model is computed from a combination of geometric factors such as clashscore, percentage of bad rotamers and unfavorable Ramachandran percentage (Chen *et al.*, 2010). The resultant value is intended to reflect an estimate of the data resolution for the model. On average, a w_A value of 1.0 is a good balance between the R_{free}- and *MolProbity*-based geometry scores. The R_{free} did suggest a tendency to favor higher w_A values in the case of low-resolution data (<2.5 Å), although this coincides with elevated *MolProbity* scores that may not justify the trade-off. Increasing or decreasing the weight by more than an order of magnitude leads to underfitting or overfitting of the data and conservative or poor geometry scores, respectively. The exception to this trend (2r4r) refined to a 2.5% lowered R_{free} value using a weight of 100.0. However, this also led to increased overfitting (as monitored by the gap between R and R_{free}, which more

Table 1
Refinement results for a low-resolution crystal structure (PDB entry 3crw) using either the automatic weighting scheme (equation 2) or a weight of 1.0.

MolProbity scores reflect an estimate of the data resolution and percentile scores are given in parentheses. See §2 for details of refinements. For a table of results over all structures, see Table 2.

Method	w_A	R_{free} (%)	*MolProbity* score	R.m.s.d. bonds (Å)	R.m.s.d. angles (°)	% of hydrogen bonds
PDB	—	35.40	3.05 (86)	—	—	—
PHENIX	4.9	39.95	4.78 (2)	0.027	2.68	15
	1.0	38.65	3.56 (63)	0.005	0.83	17
CNS	18.7	39.72	3.66 (57)	0.010	0.92	25
	1.0	33.60	2.83 (93)	0.004	0.60	30
REFMAC	208.3	35.71	3.62 (59)	0.012	1.37	18
FFX	1.0	31.06	2.20 (100)	0.014	2.78	32

than doubled from 4.7% to 10.2%; data not shown) and a poor *MolProbity* score, suggesting that this improvement comes at a significant cost. The insensitivity of the R_{free} to overfitting in this case may be reflective of poor model and/or data quality and suggests that R_{free}-based optimizations of the w_A (Brünger, 1992) value without considering consequences to model geometry can be misleading in some cases. The trends in R_{free} are similar to those observed for the free likelihood
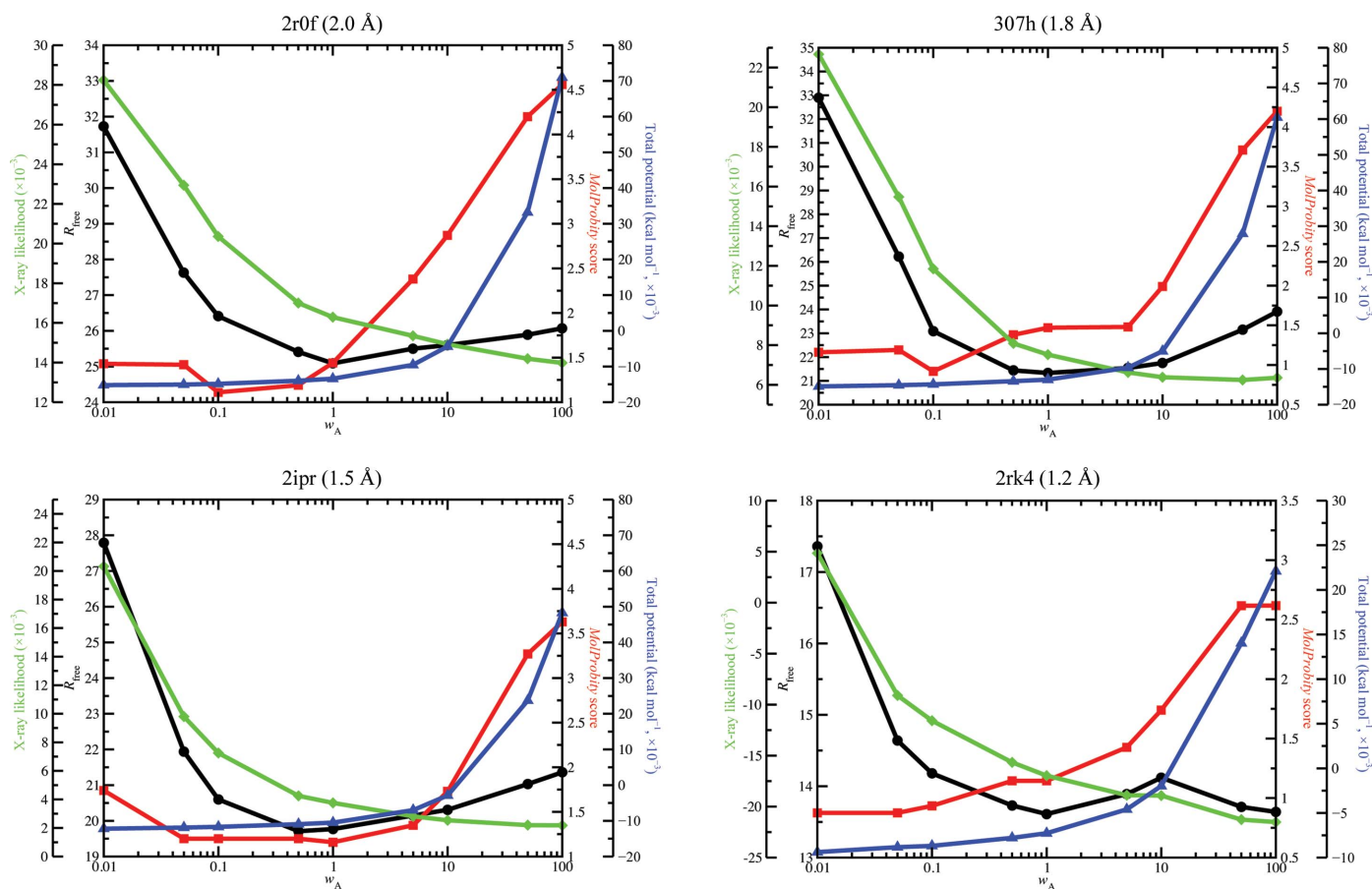
Figure 3
Plot of R_{free} (left *y* axis; black), total X-ray potential (second left *y* axis; green), *MolProbity* scores (right *y* axis; red) and total chemical potential (second right *y* axis; blue) *versus* w_A (logarithmic scale) for four representative structures ranging from 1.2 to 2.0 Å resolution (PDB entries and resolutions are given above each respective plot).

(*i.e.* the crystallographic likelihood computed for the free set of reflections; see Supplementary Figs. 1 and 2[1]), suggesting that the potential effect of 'unweighted' statistics is negligible (Ford & Rollett, 1970).

The finding that a w_A value of 1.0 is transferable across resolutions and leads to a good balance between model geometry and agreement with the data should extend to other refinement engines that employ maximum-likelihood-based targets. To illustrate this and compare it with the effect of automatic weighting, we refined this group of structures using either the weighting scheme outlined in (2) or using a static weight of 1.0 using the OPLS-AA-X force field as implemented in *CNS* v.1.3. Following refinement, we compared the resultant *MolProbity* metrics and differences between R_{free} and R (as a measure of overfitting) as a function of model resolution and the results are presented in Fig. 4. With low-resolution data (Figs. 4*a* and 4*c*), the automatic weighting scheme leads to systematic increases in *MolProbity* scores (note the gap between the green diamonds and the blue triangles in Fig. 4*c*) and overfitting (as illustrated by the gap between the black circles and the red squares in Fig. 4*a*) *versus* a static weight of 1.0. At higher resolution (approximately 2.5 Å and higher; Figs. 4*b* and 4*d*), the *MolProbity* scores using either a static or automatic weight are in close agreement, while the trend in overfitting is reversed (note the inversion in the relationship between the black circles and the red squares in Figs. 4*a* and 4*b* and the convergence between the green and blue data points between Figs. 4*c* and 4*d*). This follows the hypothesis presented earlier: high-resolution data sets will lead to systematically low weighting of the data, while at low resolution the trend is reversed, leading to significant overfitting and poor model geometry. This is also apparent in the w_A values themselves (shown in magenta).

In the case of low-resolution data, the crystallographic likelihood target will be relatively flat and contains less information. This leads to a strong dependence on the atomic forces provided by the force field to augment the refinement of models against such diffraction data. Therefore, it is critical that the force field is accurate and transferable for the resultant model to agree with the data and expectations based on our established understanding of chemistry and electrostatics. Although fixed-charge force fields, such as those used in *CNS*, have been tuned over many years, their lack of an explicit treatment of electronic polarization limits their transferability between vacuum and condensed phases (Ponder & Case, 2003; Lopes *et al.*, 2009). For example, incorporation of electrostatic effects in the force field should lead to stable hydrogen bonding and thereby improve atomic positioning. Such hydrogen bonding defines secondary-structural motifs such as β-sheets, which provide a test case for this hypothesis. This is illustrated in Fig. 5 for a 4 Å model refined using automatic weighting and Engh and Huber (EH) based restraints (Engh & Huber, 1991; Vagin *et al.*, 2004) as implemented in *PHENIX*

---

[1] Supplementary material has been deposited in the IUCr electronic archive (Reference: DZ5236). Services for accessing this material are described at the back of the journal.

Table 2
Average refinement results for 17 crystal structures using either the automatic weighting scheme (equation 2) or a weight of 1.0.

One of the 18 models used in Fig. 4 (2rk4) was omitted owing to the presence of anisotropic temperature factors, which are not available in *CNS*-based refinements. *MolProbity* scores reflect an estimate of the data resolution and percentile scores are given in parentheses. See §2 for details of refinements.

Resolution (Å)	Method	w_A	R (%)	R_{free} (%)	*MolProbity* score	R.m.s.d. bonds (Å)	R.m.s.d. angles (°)
2.68	PDB	—	23.58	27.65	2.95 (53)	—	—
	PHENIX	7.4	21.44	29.27	3.19 (39)	0.022	2.20
		1.0	21.73	29.71	2.36 (80)	0.004	0.80
	CNS	5.6	24.07	30.06	2.70 (67)	0.008	0.84
		1.0	26.49	29.84	2.37 (84)	0.005	0.63
	REFMAC	2.3	19.55	29.76	2.54 (73)	0.015	1.52
	FFX	1.0	21.57	27.51	1.96 (95)	0.013	2.61

(Adams *et al.*, 2010; Figs. 5*a* and 5*c*) or a w_A of 1.0 and the AMOEBA force field as implemented in *FFX* (Figs. 5*b* and 5*d*). Protein main-chain atoms resulting from refinements using the EH-based restraints alone (Fig. 5*a*) are significantly shifted such that hydrogen bonds are weak or not formed at all. For example, the amino acid at the upper leftmost position in Fig. 5(*a*) rotates out of the β-sheet plane and is therefore no longer properly positioned to form a hydrogen-bond interaction. These factors negatively influence the resultant *MolProbity* scores and the percentage of calculated intramolecular hydrogen bonds, and lead to poor agreement with the data regardless of the weighting scheme employed for this test model using EH-based methods (Table 1). These results are consistent with respect to the models selected, as reflected in the averages across the test set (Table 2). Use of a fixed-charge OPLS-AA force field with conditionally convergent electrostatics (as implemented in *CNS*) shows some improvement over the EH-based results (Table 1). The AMOEBA model as implemented in *FFX* improves the *MolProbity*-based effective model resolution by up to 2.5 Å and improves the agreement with the data as indicated by lower R_{free} values. Also, hydrogen bonds are more regular in terms of distance (*i.e.* closer to the canonical 1.96 Å separation) and N—H—O angle (approximately 165°, compare Figs. 5*c* and 5*d*) in the β-sheet structure (Baker & Hubbard, 1984; Fabiola *et al.*, 1997). The electron density is too weak to explicitly determine the locations of these atoms (Supplementary Fig. 3[1]). The angular energetics of hydrogen bonding are properly modeled in the *FFX* case primarily owing to the polarizable atomic multipole description of the molecular electrostatics. For an extensive comparison of AMOEBA hydrogen-bonding energy, distance and orientational dependence compared with OPLS-AA and MP2/aug-cc-pvTZ electronic calculations, see Ren *et al.* (2011). These results are in agreement with other tests of the effect of electrostatics on macromolecular refinement (Schnieders *et al.*, 2011; Fenn *et al.*, 2011).

4. Conclusions

Evaluation of the X-ray refinement of macromolecular structures is complicated by the lack of a global measure of

both model quality and agreement with the data. The crystallographer is ultimately responsible for *post facto* analysis of the resultant model to assess the trade-offs between emphasizing geometry relative to R/R_{free} values and alter, if necessary, the weighting between the chemical and data-based potentials to eventually find an optimum balance. Furthermore, this process is subjective and prone to error and/or misinterpretation. Equation (2) is intended to alleviate this necessity by upweighting the weaker potential; however, this is not desirable in a maximum-likelihood context where the data-based potential is naturally weighted by the model and data uncertainty. We therefore sought to further analyze this problem, particularly in the context of polarizable force fields, where the chemical potential is more accurate and transferable than in the canonical Engh and Huber/CIF-based methods (Engh & Huber, 1991; Vagin *et al.*, 2004) or fixed-charge force fields (Ponder & Case, 2003).

The automatic weighting scheme described by (2) led to a resolution-dependent weight that overweights low-resolution diffraction data (*i.e.* $w_A > 1.0$), causing increased overfitting

and poor geometry scores (Figs. 4*a* and 4*c*). In the opposing extreme of high-resolution data (>2.0 Å), the automatic weights led to underfitting (*i.e.* $w_A < 1.0$) coupled with conservative *MolProbity* scores (Figs. 4*b* and 4*d*). In the case of *FFX*, refinement of a variety of structures ranging from 1.2 to 4.0 Å resolution across a number of w_A values using AMOEBA chemical forces and a likelihood target for the data (see §2) suggest that a w_A of 1.0 tends to yield optimum geometric scores and R_{free} values (Figs. 2 and 3), which is on the order of our prediction of kT based on Bayes' law. The inherent weighting of the crystallographic data by the likelihood function coupled with a polarizable force field essentially eliminates the need for varying the weight compared with previous-generation refinement methods.

The importance of congruence between the chemical and data-based potentials is particularly problematic with respect to low-resolution diffraction data. In such cases, prior chemical information that does not accurately reproduce atomic forces, such as hydrogen bonding as described by polarizable electrostatics, will lead to poor model quality
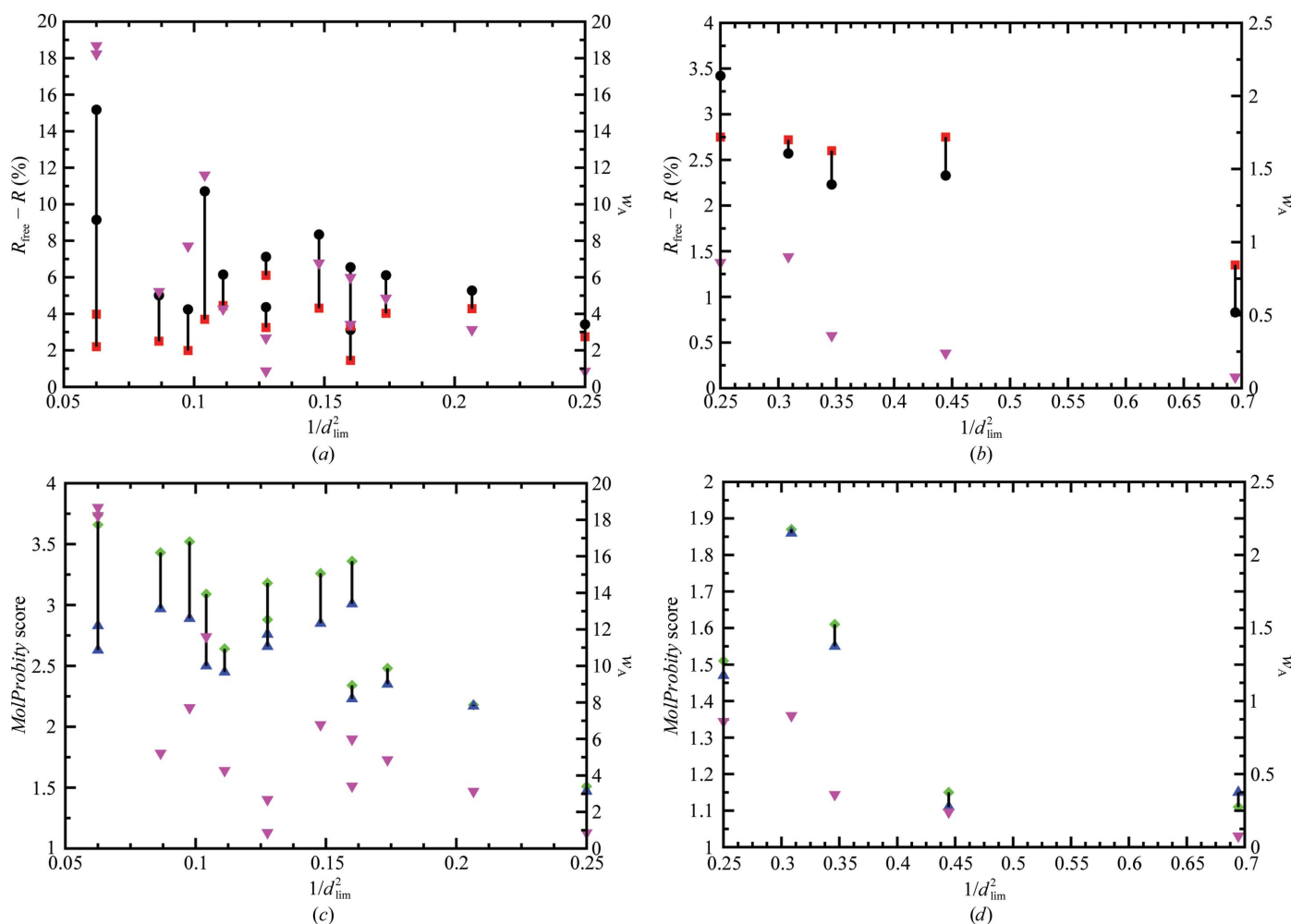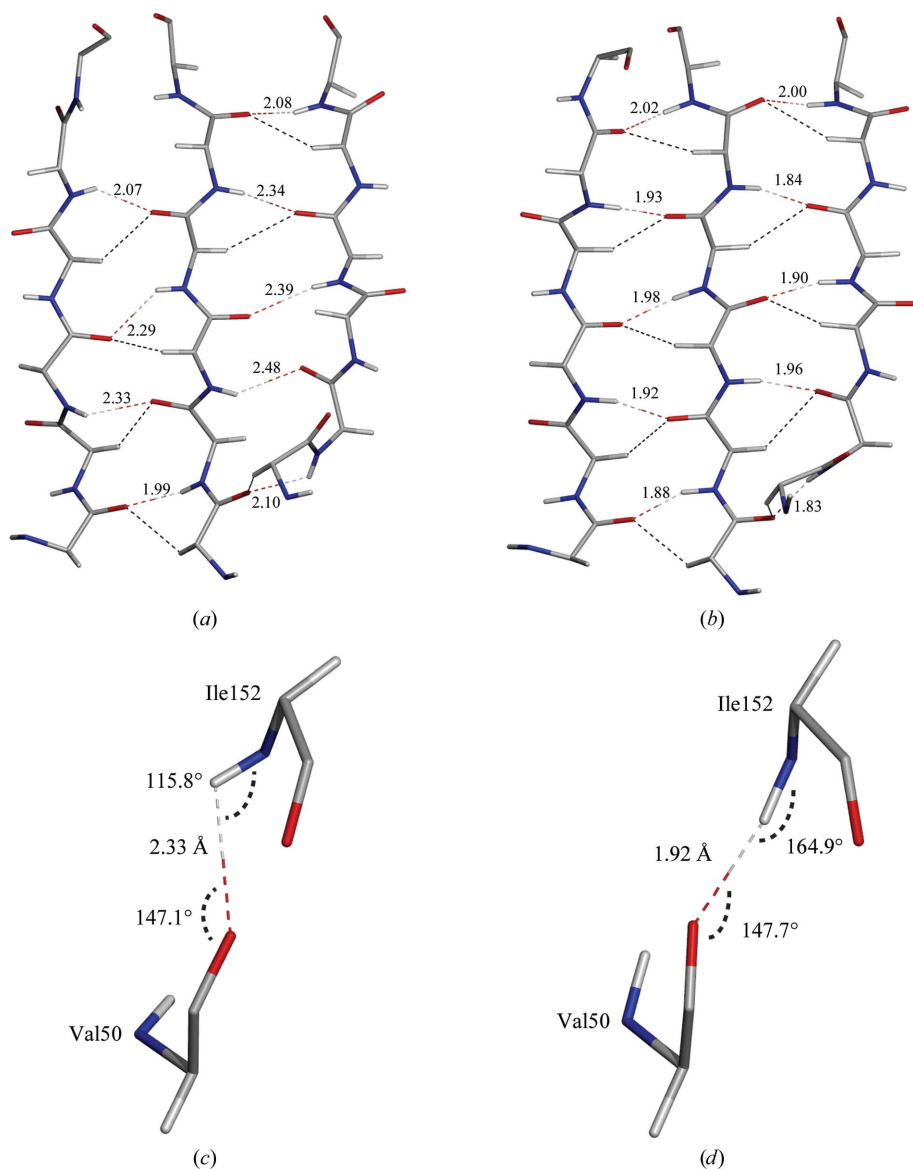

Figure 4
Plot of $R_{\text{free}} - R$ and *MolProbity* scores as a function of resolution. Black and red points refer to $R_{\text{free}} - R$ differences (*a* and *b*) using either the automatic weight (black circles) or a w_A of 1.0 (red squares), while green and blue points refer to *MolProbity* scores (*c* and *d*) using either the automatic weight (green diamonds) or a w_A of 1.0 (blue triangles). Black lines are drawn connecting the automatic weight values with those obtained using a weight of 1.0. The automatically determined w_A values themselves are also shown as magenta triangles. (*a*) and (*c*), structures ranging from 2.5 to 4.0 Å resolution. (*b*) and (*d*), structures ranging from 1.2 to 2.5 Å resolution.

because this information is weak or absent in the crystallographic likelihood target. A significant body of methodology has been directed at this problem, including elastic networks (Schroder *et al.*, 2010; Murshudov *et al.*, 2011), conformationally dependent libraries (Berkholz *et al.*, 2009; Tronrud *et al.*, 2010), studies of τ angles (Touw & Vriend, 2010) and hydrogen-bond restraints (Fabiola *et al.*, 2002; Echols *et al.*, 2010). Rather than add/reparameterize non-electrostatic based restraints to correct for the neglect of electrostatics or to augment inherently limited fixed-charge electrostatics, we believe the polarizable atomic multipole AMOEBA force field represents a more fundamental solution. The AMOEBA model has been systematically designed to reproduce the quantum-mechanical potential energy surface in vacuum and, *via* polarization, experimental condensed phase properties including densities and heats of vaporization (Ren & Ponder, 2003, 2004; Jiao *et al.*, 2008; Ponder *et al.*, 2010; Ren *et al.*, 2011). On the other hand, it is not at all clear that the energetic sum of bond and angle restraints coupled to an Engh and Huber van der Waals nonbonded term, which has been further augmented by additional *ad hoc* restraints, is able to replicate the quantum-mechanical potential energy surface or any other well defined target. As an example, protein hydrogen bonds commonly occur through the free electron pairs of carbonyl O atoms, which have a nonlinear angle and distance dependence with respect to the hydrogen-bond donor (Baker & Hubbard, 1984; Fabiola *et al.*, 1997). This is illustrated in Fig. 5, where the *FFX* model properly captures the expected angle/distance for both interacting lone-pair electrons (Fig. 5*d*), primarily as a result of the quadrupole description of the electrostatic potential around the carbonyl O atom. This bifurcated hydrogen bonding is an essential component in recapitulating twist and shear effects in β-sheet structures (Ho & Curmi, 2002). Standard *PHENIX* refinement without electrostatics (Fig. 5*c*), atom-centered fixed-charge force fields and spring-based restraints (*e.g.* hydrogen-bond restraints; Echols *et al.*, 2010) cannot capture the well defined angular dependence of this effect (Morozov *et al.*, 2004) and therefore depends completely on the experimental data to provide this information. At low resolution, however, this information is weak or absent.

As hardware and software improve to enable the collection of data sets from crystals spanning an increasingly wider resolution range over increasingly complex conditions, the description and weighting of the chemical target term must be robust and transferable across varying environments to precisely recapitulate the atomic positions and forces that are present in the crystal. The limitations and difficulties of current methods and weighting schemes in dealing with these issues has been touched upon in the past (Jack & Levitt, 1978; Lebedev *et al.*, 2003; McCoy, 2004; Afonine *et al.*, 2005*a*; Read, 2010). We suggest that the combination of a modern polarizable force field with a statically weighted maximum-likelihood crystallographic target yields robust state-of-the-art biomolecular models

Figure 5
Three-stranded β-sheet domain in 3crw (4.0 Å resolution). (*a*) Refinement results using *PHENIX* and the automatic weighting scheme. (*b*) Refinement using *FFX* and a weight of 1.0. β-Sheet hydrogen bonds are shown as dashed lines, with N—H···O hydrogen bonds shown in red and white with distances in Å provided above them. Black dashed lines refer to 'weak' C^α—H···O hydrogen bonds that are also an important factor in β-sheet structure (Ho & Curmi, 2002). (*c*) Detail of one hydrogen bond showing angle and distance values from *PHENIX* refinement. (*d*) Detail of the same hydrogen bond as in (*c*) with values from *FFX*-based refinement.

with increased information content. Furthermore, this approach alleviates the crystallographer from the burden of choosing the weighting factor manually and serves as a general approach for crystallographic model refinement.

References

Adams, P. D. *et al.* (2010). *Acta Cryst.* D**66**, 213–221.
Adams, P. D., Pannu, N. S., Read, R. J. & Brünger, A. T. (1997). *Proc. Natl. Acad. Sci. USA*, **94**, 5018–5023.
Afonine, P. V., Grosse-Kunstleve, R. W. & Adams, P. D. (2005*a*). *CCP4 Newsl. Protein Crystallogr.* **42**, 43–49.
Afonine, P. V., Grosse-Kunstleve, R. W. & Adams, P. D. (2005*b*). *Acta Cryst.* D**61**, 850–855.
Arendall, W. B. III, Tempel, W., Richardson, J. S., Zhou, W., Wang, S., Davis, I. W., Liu, Z.-J., Rose, J. P., Carson, W. M., Luo, M., Richardson, D. C. & Wang, B.-C. (2005). *J. Struct. Funct. Genomics*, **6**, 1–11.
Baker, E. N. & Hubbard, R. E. (1984). *Prog. Biophys. Mol. Biol.* **44**, 97–179.
Berkholz, D. S., Shapovalov, M. V., Dunbrack, R. L. & Karplus, P. A. (2009). *Structure*, **17**, 1316–1325.
Bhattacharya, A., Tejero, R. & Montelione, G. T. (2007). *Proteins*, **66**, 778–795.
Bricogne, G. (2006). *International Tables for Crystallography*, Vol. *B, Reciprocal Space*, 1st online ed., edited by U. Shmueli, pp. 25–98. Chester: International Union of Crystallography.
Brünger, A. T. (1988). *J. Mol. Biol.* **203**, 803–816.
Brünger, A. T. (1989). *Acta Cryst.* A**45**, 42–50.
Brünger, A. T. (1992). *Nature (London)*, **355**, 472–475.
Chen, V. B., Arendall, W. B., Headd, J. J., Keedy, D. A., Immormino, R. M., Kapral, G. J., Murray, L. W., Richardson, J. S. & Richardson, D. C. (2010). *Acta Cryst.* D**66**, 12–21.
Cowtan, K. (2002). *J. Appl. Cryst.* **35**, 655–663.
Cowtan, K. (2005). *J. Appl. Cryst.* **38**, 193–198.
Darden, T., York, D. & Pedersen, L. (1993). *J. Chem. Phys.* **98**, 10089–10092.
Echols, N., Headd, J. J., Afonine, P. & Adams, P. D. (2010). *Comput. Crystallogr. Newsl.* **1**, 12–17.
Engh, R. A. & Huber, R. (1991). *Acta Cryst.* A**47**, 392–400.
Essmann, U., Perera, L., Berkowitz, M. L., Darden, T., Lee, H. & Pedersen, L. G. (1995). *J. Chem. Phys.* **103**, 8577–8593.
Fabiola, F., Bertram, R., Korostelev, A. & Chapman, M. S. (2002). *Protein Sci.* **11**, 1415–1423.
Fabiola, G. F., Krishnaswamy, S., Nagarajan, V. & Pattabhi, V. (1997). *Acta Cryst.* D**53**, 316–320.
Faver, J. C., Benson, M. L., He, X., Roberts, B. P., Wang, B., Marshall, M. S., Sherrill, C. D. & Merz, K. M. Jr (2011). *PLoS One*, **6**, e18868.
Fenn, T. D., Schnieders, M. J. & Brunger, A. T. (2010). *Acta Cryst.* D**66**, 1024–1031.
Fenn, T. D., Schnieders, M. J., Brunger, A. T. & Pande, V. S. (2010). *Biophys. J.* **98**, 2984–2992.
Fenn, T. D., Schnieders, M. J., Mustyakimov, M., Wu, C., Langan, P., Pande, V. S. & Brunger, A. T. (2011). *Structure*, **19**, 523–533.
Ford, G. C. & Rollett, J. S. (1970). *Acta Cryst.* A**26**, 162.
Habeck, M., Rieping, W. & Nilges, M. (2006). *Proc. Natl. Acad. Sci. USA*, **103**, 1756–1761.
Ho, B. K. & Curmi, M. G. (2002). *J. Mol. Biol.* **317**, 291–308.
Jack, A. & Levitt, M. (1978). *Acta Cryst.* A**34**, 931–935.
Jiao, D., Golubkov, P. A., Darden, T. A. & Ren, P. (2008). *Proc. Natl. Acad. Sci. USA*, **105**, 6290–6295.
Jorgensen, W. L. & Tirado-Rives, J. (1988). *J. Am. Chem. Soc.* **110**, 1657–1666.
Lebedev, A. A., Tickle, I. J., Laskowski, R. A. & Moss, D. S. (2003). *Acta Cryst.* D**59**, 1557–1566.
Linge, J. P., Williams, M. A., Spronk, C. A., Bonvin, A. M. & Nilges, M. (2003). *Proteins*, **50**, 496–506.
Lopes, P. E., Roux, B. & Mackerell, A. D. (2009). *Theor. Chem. Acc.* **124**, 11–28.
McCoy, A. J. (2004). *Acta Cryst.* D**60**, 2169–2183.
Morozov, A. V., Kortemme, T., Tsemekhman, K. & Baker, D. (2004). *Proc. Natl. Acad. Sci. USA*, **101**, 6946–6951.
Murshudov, G. N., Skubák, P., Lebedev, A. A., Pannu, N. S., Steiner, R. A., Nicholls, R. A., Winn, M. D., Long, F. & Vagin, A. A. (2011). *Acta Cryst.* D**67**, 355–367.
Murshudov, G. N., Vagin, A. A. & Dodson, E. J. (1997). *Acta Cryst.* D**53**, 240–255.
Nozinovic, S., Fürtig, B., Jonker, H. R., Richter, C. & Schwalbe, H. (2010). *Nucleic Acids Res.* **38**, 683–694.
Panigrahi, S. K. & Desiraju, G. R. (2007). *J. Biosci.* **32**, 677–691.
Ponder, J. W. & Case, D. A. (2003). *Adv. Protein Chem.* **66**, 27–85.
Ponder, J. W., Wu, C., Ren, P., Pande, V. S., Chodera, J. D., Schnieders, M. J., Haque, I., Mobley, D. L., Lambrecht, D. S., DiStasio, R. A., Head-Gordon, M., Clark, G. N., Johnson, M. E. & Head-Gordon, T. (2010). *J. Phys. Chem. B*, **114**, 2549–2564.
Read, R. J. (2010). *Structure*, **18**, 664–665.
Ren, P. & Ponder, J. W. (2003). *J. Phys. Chem. B*, **107**, 5933–5947.
Ren, P. & Ponder, J. W. (2004). *J. Phys. Chem. B*, **108**, 13427–13437.
Ren, P., Wu, C. & Ponder, J. W. (2011). *J. Chem. Theor. Comput.*, doi:10.1021/ct200304d.
Sagui, C., Pedersen, L. G. & Darden, T. A. (2004). *J. Chem. Phys.* **120**, 73–87.
Schnieders, M. J., Fenn, T. D. & Pande, V. S. (2011). *J. Chem. Theor. Comput.* **7**, 1141–1156.
Schnieders, M. J., Fenn, T. D., Pande, V. S. & Brunger, A. T. (2009). *Acta Cryst.* D**65**, 952–965.
Schröder, G. F., Levitt, M. & Brunger, A. T. (2010). *Nature (London)*, **464**, 1218–1222.
Ten Eyck, L. F. (1973). *Acta Cryst.* A**29**, 183–191.
Ten Eyck, L. F. (1977). *Acta Cryst.* A**33**, 486–492.
Touw, W. G. & Vriend, G. (2010). *Acta Cryst.* D**66**, 1341–1350.
Tronrud, D. E., Berkholz, D. S. & Karplus, P. A. (2010). *Acta Cryst.* D**66**, 834–842.
Vagin, A. A., Steiner, R. A., Lebedev, A. A., Potterton, L., McNicholas, S., Long, F. & Murshudov, G. N. (2004). *Acta Cryst.* D**60**, 2184–2195.
Wang, H. & Stubbs, G. (1993). *Acta Cryst.* A**49**, 504–513.
Waser, J. (1955). *Acta Cryst.* **8**, 595.